EBioMedicine 11 (2016) 253–261

Contents lists available at ScienceDirect

EBioMedicine

journal homepage: www.ebiomedicine.com

Research Paper

Nitric Oxide-induced Activation of the Type 1 Ryanodine Receptor Is Critical for Epileptic Seizure-induced Neuronal Cell Death

Yoshinori Mikami [a,b], Kazunori Kanemaru [a], Yohei Okubo [a], Takuya Nakaune [a], Junji Suzuki [a], Kazuki Shibata [c], Hiroki Sugiyama [c], Ryuta Koyama [c], Takashi Murayama [d], Akihiro Ito [e,f], Toshiko Yamazawa [g], Yuji Ikegaya [c], Takashi Sakurai [d], Nobuhito Saito [e], Sho Kakizawa [h,*], Masamitsu Iino [a,i,*]

[a] Department of Pharmacology, Graduate School of Medicine, The University of Tokyo, 7-3-1 Hongo, Bunkyo-ku, Tokyo 113-0033, Japan
[b] Department of Physiology, School of Medicine, Faculty of Medicine, Toho University, 5-21-16 Omori-Nishi, Ota-ku, Tokyo 143-8540, Japan
[c] Laboratory of Chemical Pharmacology, Graduate School of Pharmaceutical Sciences, The University of Tokyo, 7-3-1 Hongo, Bunkyo-ku, Tokyo 113-0033, Japan
[d] Department of Pharmacology, Graduate School of Medicine, Juntendo University, 2-1-1 Hongo, Bunkyo-ku, Tokyo 113-8421, Japan
[e] Department of Neurosurgery, Graduate School of Medicine, The University of Tokyo, 7-3-1 Hongo, Bunkyo-ku, Tokyo 113-8655, Japan
[f] Department of Neurosurgery, Graduate School of Medicine, Teikyo University, 2-11-1 Kaga, Itabashi-Ku, Tokyo 117-003, Japan
[g] Department of Molecular Physiology, The Jikei University School of Medicine, 3-25-8 Nishishimbashi, Minato-ku, Tokyo 105-8461, Japan
[h] Department of Biological Chemistry, Graduate School of Pharmaceutical Sciences, Kyoto University, 46-29 Yoshida-Shimoadachi-cho, Sakyo-ku, Kyoto 606-8501, Japan
[i] Department of Cellular and Molecular Pharmacology, Nihon University School of Medicine, 30-1 Oyaguchi Kami-cho, Itabashi-ku, Tokyo 173-8610, Japan

ARTICLE INFO

Article history:
Received 23 March 2016
Received in revised form 5 August 2016
Accepted 12 August 2016
Available online 13 August 2016

Keywords:
Ryanodine receptor
Nitric oxide
Calcium
Seizures
Neurodegeneration

ABSTRACT

Status epilepticus (SE) is a life-threatening emergency that can cause neurodegeneration with debilitating neurological disorders. However, the mechanism by which convulsive SE results in neurodegeneration is not fully understood. It has been shown that epileptic seizures produce markedly increased levels of nitric oxide (NO) in the brain, and that NO induces Ca^{2+} release from the endoplasmic reticulum *via* the type 1 ryanodine receptor (RyR1), which occurs through *S*-nitrosylation of the intracellular Ca^{2+} release channel. Here, we show that through genetic silencing of NO-induced activation of the RyR1 intracellular Ca^{2+} release channel, neurons were rescued from seizure-dependent cell death. Furthermore, dantrolene, an inhibitor of RyR1, was protective against neurodegeneration caused by SE. These results demonstrate that NO-induced Ca^{2+} release *via* RyR is involved in SE-induced neurodegeneration, and provide a rationale for the use of RyR1 inhibitors for the prevention of brain damage following SE.

© 2016 The Authors. Published by Elsevier B.V. This is an open access article under the CC BY-NC-ND license (http://creativecommons.org/licenses/by-nc-nd/4.0/).

1. Introduction

Epilepsy is caused by a wide variety of insults to the brain as well as by congenital abnormalities in ionic channels (Berkovic et al., 2006; Jentsch et al., 2004; Meisler and Kearney, 2005). Status epilepticus (SE) is a neurological emergency and results in brain damage that increases the risk of recurrent seizures and debilitating neuronal abnormalities including death (Chang and Lowenstein, 2003; Goldberg and Coulter, 2013). Its high morbidity and mortality makes SE one of the most significant neurological disorders in terms of high social costs (Betjemann and Lowenstein, 2015). Therefore, understanding of the pathophysiology of SE-induced brain damage is required for the treatment of the neurological emergency. During epileptic seizures, NO formation has been observed to increase as a result of Ca^{2+}-dependent activation of NO synthase (NOS) in neurons (Mülsch et al., 1994). This increase in NO levels has been implicated in seizure-induced neuronal cell loss based on the finding that neurodegeneration is attenuated in neuronal NOS (nNOS)-deficient mice (Parathath et al., 2007). Thus NO is strongly implicated as a neurodegenerative factor in epileptic states. However, the molecular mechanisms by which NO exerts its role in SE-induced neurodegeneration requires clarification. Thus, rational treatment for the prevention of brain damage associated with SE has yet to be explored.

In addition to the cyclic guanosine monophosphate-dependent protein kinase pathway, NO is known to regulate the function of target proteins through *S*-nitrosylation of cysteine residues (Hess et al., 2005; Jaffrey et al., 2001). One such target is the type 1 ryanodine receptor (RyR1), which is the Ca^{2+}-induced Ca^{2+} release (CICR) channel in the endoplasmic reticulum (ER). NO induces the opening of the RyR1 channel through *S*-nitrosylation (Aghdasi et al., 1997; Eu et al., 2000; Sun et al., 2001). The activity of RyR1 due to this activation mechanism has been implicated in Ca^{2+} leakage from skeletal muscle Ca^{2+} stores that has been attributed to certain pathological conditions (Bellinger et al., 2009; Durham et al., 2008). A single cysteine residue at 3635 (C3635)

* Corresponding authors.
E-mail addresses: kakizawa.sho.4u@kyoto-u.ac.jp (S. Kakizawa), iino@m.u-tokyo.ac.jp (M. Iino).

http://dx.doi.org/10.1016/j.ebiom.2016.08.020
2352-3964/© 2016 The Authors. Published by Elsevier B.V. This is an open access article under the CC BY-NC-ND license (http://creativecommons.org/licenses/by-nc-nd/4.0/).

in rabbit RyR1 is responsible for sensitizing the skeletal muscle Ca^{2+} release channel to NO (Sun et al., 2001). An alanine substitution for C3635 (C3635A) of RyR1 expressed in human embryonic kidney (HEK) 293 cells has been shown to reduce *S*-nitrosylation levels and abolish the regulation of the skeletal muscle Ca^{2+}-release channel by physiological concentrations of NO (Sun et al., 2001). In the brain, NO induces Ca^{2+} release from the ER through *S*-nitrosylation of RyR1, which results in an increased concentration of intracellular Ca^{2+} in neurons (Kakizawa et al., 2012). Ca^{2+} release *via* RyR1 has also been implicated in NO-induced neuronal cell death, as shown by studies in which cell death is significantly milder in cultured neurons taken from RyR1-deficient mice than in controls (Kakizawa et al., 2012). These studies raise the possibility that NO-induced Ca^{2+} release (NICR) is involved in certain pathological states in the brain; however, the pathophysiological role of NICR remains to be established. Furthermore, pathophysiological significance of NICR *in vivo* has not been examined.

In this study, we examined whether NICR *via S*-nitrosylated RyR1 is involved in SE-induced neurodegeneration. In order to study the role of NICR *in vivo*, we generated a knock-in mouse line, in which the essential cysteine residue at 3636 of mouse RyR1 (corresponding to cysteine 3635 in humans and rabbits) was replaced by alanine (*Ryr1*^{C3636A}) to prevent its *S*-nitrosylation. We show that NICR was indeed silenced in neurons from *Ryr1*^{C3636A} knock-in mice, which allowed us to examine the role of NICR in a kainic acid (KA)-model of temporal lobe epilepsy. Here we provide evidence that NICR exacerbates neurodegeneration in the hippocampus following KA-induced seizures, suggesting that RyR1 is a promising therapeutic target candidate to ameliorate the neurodegenerative effect of SE.

2. Materials and Methods

2.1. Chemicals

3-[(3-cholamidopropyl)dimethylammonio]-1-propanesulfonate (CHAPS), D(+)-glucose, ethanol, 2-[4-(2-Hydroxyethyl)-1-piperazinyl]ethanesulfonic acid (HEPES), magnesium chloride, *N*-ethylmaleimide (NEM), Nonidet P 40 (NP-40), potassium permanganate, sodium chloride, sodium dodecylsulfate (SDS) and tris(hydroxymethyl)aminomethane were purchased from Nacalai Tesque (Kyoto, Japan). Calcium chloride dehydrates, dantrolene sodium salt, L-glutamic acid, β-mercaptoethanol, neocuproine and TritonX-100 were purchased from Sigma-Aldrich (St. Louis, MO, USA). Acetic acid, acetone, caffeine, dithiothreitol (DTT) and potassium chloride were purchased from Wako Pure Chemicals (Osaka, Japan). Calcein-AM, 4′-6-diamidino-2-phenylindole (DAPI) solution, ethylenediaminetetraacetic acid (EDTA), Hoechst33342, 1-hydroxy-2-oxo-3-(*N*-methyl-3-aminopropyl)-3-methyl-1-triazene (NOC7), 3-morpholinosydnonimine (SIN-1), were purchased from Dojindo (Kumamoto, Japan). Kainic acid (KA), (5*S*,10*R*)-(+)-5-Methyl-10,11-dihydro-5*H*-dibenzo[*a*,*d*]cyclohepten-5,10-imine maleate (MK-801) and *N*-methyl-D-aspartate (NMDA) were purchased from Tocris Bioscience (Bristol, UK).

2.2. Animals

All animal-related procedures were in accordance with the guidelines of the University of Tokyo. Mice were housed in a transparent plastic cage, fed with food and water *ad libitum*, and kept under controlled lighting conditions (12 h-light/12 h-dark) in specific pathogen-free conditions in the University of Tokyo animal facility. The maximum number of adult mice in a cage was 7. The *Ryr1*$^{+/C3636A}$ knock-in mouse was generated at UNITECH (Kashiwa, Japan). Briefly, the targeting vector contained genomic DNA encompassing exon 74 of the mouse *Ryr1* gene with a nucleotide change encoding for the mutation at codon 3636 (TGT → GCT, C3636A). The targeting vector was transfected into embryonic stem (ES) cells, and targeted ES clones were screened and confirmed by Southern analysis. The correctly targeted ES cells were injected into blastocysts to generate chimeric mice. Mice carrying the targeted allele were crossed with Tg-Cre transgenic mice to remove the floxed neomycin cassette and produce heterozygous *Ryr1*$^{+/C3636A}$ mice. Crossing of heterozygous *Ryr1*$^{+/C3636A}$ mice yielded homozygous *Ryr1*$^{C3636A/C3636A}$ mice, designated as *Ryr1*^{C3636A} mice.

The primer sequences for genotyping were as follows: forward, 5′-GCTTAAGGACTGGACATAGAGCTAA-3′; and reverse, 5′-CTGAATATGTGGATATGGGTATAGG-3′. PCR was conducted using *Thermococcus kodakaraensis* (KOD-FX) DNA polymerase (Toyobo, Osaka, Japan) with the following amplification cycle: 94 °C for 1 min followed by 40 cycles of 94 °C for 10 s and 68 °C for 1 min. The 471 and/or 361 bp bands were detected by 2.5% (*w*/*v*) agarose gel electrophoresis stained with ethidium bromide.

2.3. Preparation of Cerebral Neuronal Culture

Neurons were prepared from the cerebral cortices of mice fetuses (postnatal day 0) based on a modification of a previously described procedure (Kakizawa et al., 2012; Kanemaru et al., 2007). Briefly, minced cerebral cortices were treated with 1.0% (*w*/*v*) trypsin and 0.1% (*w*/*v*) Deoxyribonulease I (Sigma-Aldrich) in Ca^{2+}/Mg^{2+}-free phosphate-buffered saline (PBS) (Takara, Shiga, Japan) for 5 min at room temperature (RT). Cells were washed with Neurobasal-A medium supplemented with 5% (*v*/v) fetal bovine serum (FBS), penicillin (100 units mL^{-1}), streptomycin (100 units mL^{-1}), B-27 supplement, and 2 mM L-glutamine (Gibco, ThermoFisher Scientific, Grand Island, NY, USA) and dissociated by triturating with a fire-polished Pasteur pipette in Ca^{2+}/Mg^{2+}-free PBS containing 0.05% (*w*/*v*) Deoxyribonulease I and 0.03% (*w*/*v*) trypsin inhibitor (Sigma-Aldrich). Dispersed cells were plated at 1.0×10^5 cells cm^{-2} on glass slide coated with poly-L-lysine and laminin (Sigma-Aldrich). Cells were then cultured at 37 °C under a humidified atmosphere containing 5% CO_2. The medium was changed every 2 d by replacing half of the old medium with fresh FBS-free medium. Cells cultured for 7–10 d were used for experiments.

2.4. Preparation of Skeletal Muscle Primary Culture

Primary cultured myoblasts from newborn mice were prepared based on a modification of a previously described procedure (Rando and Blau, 1994). Briefly, the forelimbs and hindlimbs were removed and bones dissected away. The muscle was cut into small fragments and enzymatically dissociated with collagenase (from *Clostridium histolyticum*, 2.5 mg mL^{-1}, Wako Pure Chemicals) at 37 °C for 15 min. The fragments were passed through 40-μm cell strainer and the suspension subjected to low-speed centrifugation. The pellet was resuspended in Dulbecco's modified Eagle medium (DMEM) supplemented with 20% (*v*/v) FBS, penicillin (100 units mL^{-1}), streptomycin (100 units mL^{-1}), 2 mM L-glutamine and 10 ng mL^{-1} recombinant human fibroblast growth factor (FGF)-basic (Gibco). Myoblasts were differentiated into myotubes with DMEM containing 2% horse serum.

2.5. Intracellular Ca^{2+} Imaging

Ca^{2+} imaging was carried out based on a modification of the previously described procedure (Kakizawa et al., 2012). Briefly, neurons and myocytes were loaded with 5 μM Fura-2 acetoxymethyl ester (Fura-2AM) (Molecular Probes, ThermoFisher Scientific, Eugene, OR, USA) for 30 min in HEPES-buffered saline (150 mM NaCl, 4 mM KCl, 2 mM $CaCl_2$, 1 mM $MgCl_2$, 5 mM HEPES, 5.6 mM glucose, pH adjusted to 7.4 with NaOH). Fluorescence images were acquired at 510 nm using an inverted microscope (IX81, Olympus, Tokyo, Japan) with a UApo/340 40× (numerical aperture (NA) 1.35; Olympus) and a cooled CCD camera (EM-CCD C9100, Hamamatsu Photonics, Shizuoka, Japan) at a rate of one frame every 3 s. Excitation wavelengths were 340 and

380 nm. Ca^{2+} imaging experiments were conducted at RT. Image analyses were carried out using ImageJ64 (National Institutes of Health, Bethesda, MD, USA). Regions of interests (ROIs) corresponding to individual cells were selected and the mean fluorescence intensity (F) of each ROI minus the background intensity was calculated for each frame to obtain F_{340}/F_{380} as an indicator of $[Ca^{2+}]_i$. In Fig. 1c and S3e, F_{340}/F_{380} was converted to $[Ca^{2+}]_i$ using the calibration equation (Grynkiewicz et al., 1985) with the K_d value of 224 nM. Myocytes were stimulated with an electrical pulse (10 V, 100 ms) using SEN-3201 stimulator (Nihonkohden, Tokyo, Japan).

2.6. NO Donor and Caffeine Application

To prepare a stock solution of NOC7 (100 mM), NOC7 was dissolved in 0.3 N NaOH. NO generation was induced by adding an appropriate amount of NOC7 stock solution to saline containing the same amount of 0.3 N HCl. After a 2-min incubation, the saline-containing NOC7 was applied to the primary culture.

Caffeine was dissolved in saline and applied to the primary culture by pipet. To ensure steady-state ER Ca^{2+} loading, cells were subjected to short application (10 s) of high potassium saline (114 mM NaCl, 40 mM KCl, 2 mM $CaCl_2$, 1 mM $MgCl_2$, 5 mM HEPES, 5.6 mM glucose, pH adjusted to 7.4 with NaOH) before caffeine was applied.

2.7. Analysis of Neuronal Cell Death

Neurons in primary culture (maintained at 37 °C) were exposed to 500 μM NOC7 or vehicle. After 5 h, cultures were stained with JC-1 (J-aggregate forming lipophilic cation 5,5′,6,6′-tetrachloro-1,1′,3,3′-tetraethylbenzimidazolcarbocyanine iodide) Mitochondrial Membrane Potential Assay Kit (Cayman Chemical, Ann Arbor, MI USA) for 10 min at RT. Fluorescence images were obtained at 515–550 nm (excitation at 480 nm) and 600 nm (excitation at 540 nm) using an inverted microscope equipped with PlanApo 60× (NA, 1.42; Olympus) objective and CCD camera. Cell viability was expressed as the intensity of red fluorescence divided by that of green fluorescence in the cell body of neurons.

To examine the morphology of neurons, cultured neurons were fixed with 4% (w/v) paraformaldehyde in PBS and permeabilized with 0.3% (v/v) Triton X-100 in PBS. After rinsing in PBS, cells were incubated with 10% (v/v) bovine serum albumin (Nakarai Tesque, Tokyo, Japan) in PBS at RT for 1 h. For immunofluorescence staining, cells were incubated overnight at 4 °C with antibody against mouse *anti*-neuronal class III β-tubulin clone TUJ1 (1:1000; Covance, Berkeley, CA; MMS-435P). The immunoreaction was visualized with secondary subclass-specific AlexaFluor 488-conjugated antiserum (Invitrogen, ThermoFisher Scientific, Eugene, OR, USA) at a dilution of 1:1000. Images were acquired with an Olympus IX81 inverted microscope equipped with a 20× objective (NA = 0.45) and a CCD camera.

2.8. Western Blotting

Anesthetized mice were decapitated and the cortical gray matter, hippocampus or skeletal muscle were dissected in ice-cold potassium phosphate buffer containing 0.32 M sucrose, 1 mM DTT, 1 mM EDTA, the protease inhibitor cocktail Complete (Roche Diagnostics, Mannheim, Germany) and calpain inhibitor I (Roche Diagnostics) using a Potter type glass homogenizer with a Teflon pestle and centrifuged for 10 min at 4 °C and 1000 × g, with a centrifuge to remove nuclei and intact cells. The supernatant was centrifuged for 10 min at 4 °C and 1300 × g to obtain post-nuclear supernatant. The supernatant were centrifuged for 10 min at 4 °C and 17,000 × g, with a high-speed refrigerated micro centrifuge to obtain cytosol and microsomal fraction. Protein quantification was performed on the supernatant using a Pierce BCA Protein Assay Kit (Thermo Fisher Scientific, Rockford, IL, USA). SDS-loading buffer, containing β-mercaptoethanol was added to the samples before heat incubation at 95 °C for 5 min. Five micrograms of protein samples were separated by SDS–PAGE on a 5–20% (w/v) gradient polyacrylamide gel (Wako Pure Chemicals) and electroblotted onto a polyvinylidene fluoride (PVDF) membrane (Bio-Rad) at 200 mA for 4 h in electrophoretic transfer cell (Bio-Rad). Membranes were blocked in TBSN (0.1% (v/v) NP-40 in tris-buffered saline) containing 5% (w/v) skim milk for 1 h at RT. The blots were incubated with either rabbit *anti*-RyR1 polyclonal antibody (Kakizawa et al., 2007) (1:1000), mouse *anti*-glyceraldehyde 3-phosphate dehydrogenase (GAPDH) monoclonal antibody (1:3000, Merck Millipore, Darmstadt, Germany; MAB374) or mouse anti-nNOS monoclonal antibody (1:250; Invitrogen,

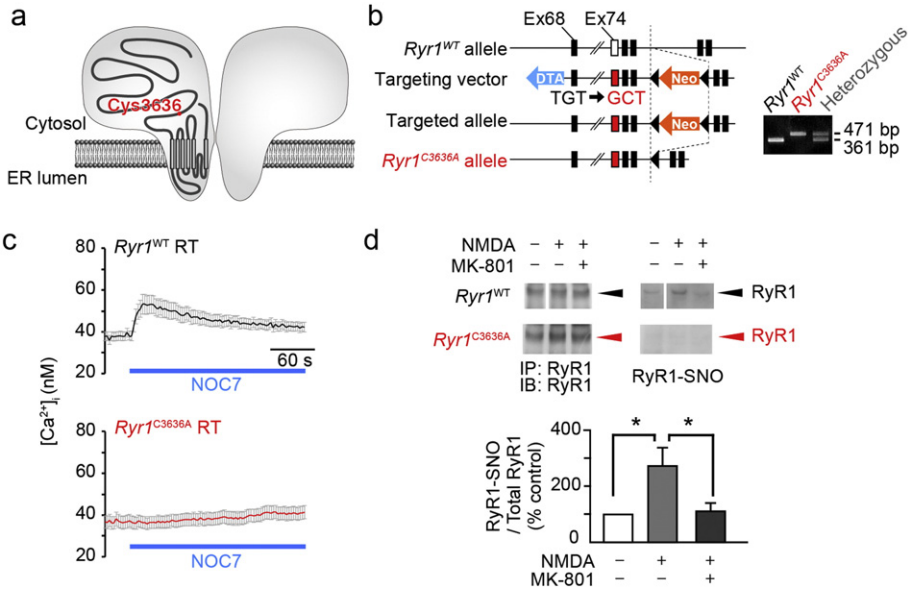

Fig. 1. Generation of *Ryr1*^{C3636A} mice and characterization of RyR1^{C3636A} channels in brain (a) Schema of the RyR1 channel. (b) Creation of *Ryr1*^{C3636A} mutant allele. (c) NOC7 (500 μM)-induced intracellular Ca^{2+} increase in *Ryr1*^{WT} and *Ryr1*^{C3636A} neurons; n = 45–67 neurons. (d) *S*-nitrosylation of RyR1 in the hippocampal slices. Bottom panel shows the levels of *S*-nitrosylated RyR1 (SNO-RyR1) in *Ryr1*^{WT} slices (n = 4). Error bars indicate s.e.m. Statistical significance was determined by analysis of variance (ANOVA) followed by a Tukey-Kramer *post-hoc* test. * $p < 0.05$. SNO-RyR1 was not detected in *Ryr1*^{C3636A} slices (n = 4). See also Fig. S1, S2 and S3.

ThermoFisher Scientific; 61-7000) in the blocking solution overnight at 4 °C. The membrane was washed in TBSN 3 times for 10 min and incubated with a horseradish peroxidase-conjugated anti-rabbit IgG (1:10,000; Medical & Biological Laboratories, Aichi, Japan) or anti-mouse IgG (1:20,000; Medical & Biological Laboratories) in TBSN for 1 h at RT. The horseradish peroxidase was visualized using Western Lightning Plus-ECL (PerkinElmer, Waltham, MA, USA) and chemiluminescence was detected using an Amersham Hyperfilm ECL film (GE Healthcare Life Sciences, Piscataway, NJ, USA).

2.9. DAR-4M Imaging

For NO imaging, NO indicator Diaminorhodamine-4M (DAR-4M) (Kojima et al., 2001) was used. Primary cultured cells were loaded with 5 μM DAR-4M AM (Sekisui Medical, Tokyo, Japan) in saline at RT for 5 min. Then time-lapse fluorescence images were captured every 3 s using the IX81 microscope.

2.10. Organotypic Cultures of Hippocampal Slices

Hippocampal organotypic slice culture was carried out based on a modification of the previously described procedure (Koyama et al., 2007; Koyama et al., 2012). Hippocampal slice cultures were prepared from *P*6–9 mice. Hippocampal slices were incubated at 37 °C in a humidified incubator with 5% CO_2 and 95% air and slices for 7–10 d *in vitro* were used for experiments.

2.11. Biotin Switch Assay

For detect the *S*-nitrosylation of RyR1, biotin switch assay was carried out based on a modification of the previously described procedure (Kakizawa et al., 2012). Hippocampal slice cultures were rinsed with HEN buffer (25 mM HEPES, pH 7.7, 0.1 mM EDTA, and 0.01 mM neocuproine). Slices were homogenized in HEN buffer containing 0.5% (*w*/*v*) CHAPS, 0.1% (*w*/*v*) SDS, 20 mM NEM, protease inhibitor cocktails Complete and calpain inhibitor I by a Potter type glass homogenizer with a Teflon pestle and lysed by rocking for 30 min at 4 °C to block sulfhydryl groups. Lysates were centrifuged at 10,000 × *g* for 10 min at 4 °C. The supernatant was recovered, supplemented with SDS at a final concentration of 1% (*w*/*v*), and further incubated for 30 min at RT to achieve complete blockade of sulfhydryl groups. Excess NEM was removed by protein precipitation with acetone, and the pellet resuspended and incubated in HEN buffer containing 1% (*w*/*v*) SDS, 10 mM ascorbic acid and *S*-Nitrosylation Labeling reagents in the kit as per manufacturer's instructions (Cayman Chemical) for reduction of *S*-nitrosothiols and labeling with biotin. Extra label was removed by a second acetone precipitation. Proteins were resuspended in lysis buffer containing 25 mM Tris-HCl, pH 7.5, 100 mM NaCl, 2 μM EDTA, 0.05% (*v*/v) TritonX-100, protease inhibitor cocktails Complete and calpain inhibitor I. For coimmunoprecipitations, 2 μL of *anti*-RyR1 polyclonal antibody (Merck Millipore; AB9078) was added to lysate and allowed to bind to the antibody for 1 h shaking at 4 °C before addition of 40 μL preequilibrated Protein G sepharose 4 FastFlow (GE Healthcare Life Science). After shaking at 4 °C for another 1 h, beads were washed 5 times in lysis buffer and bound protein was eluted at 95 °C for 5 min in 50 μL of SDS-loading buffer. Protein was separated by SDS-PAGE and electroblotted onto a PVDF membrane. Membranes were blocked in TBSN containing 3% bovine serum albumin (NakaraiTesque) for 1 h at RT. Protein was detected by immunoblotting using a polyclonal antibody against RyR1 (Kakizawa et al., 2007). The blot was then stripped and re-probed with streptavidin-HRP (horse radish peroxidase; Sigma-Aldrich) by chemiluminescence to identify *S*-nitrosylation of RyR1. *S*-nitrosylated RyR1 was normalized by the intensity of the RyR1 band.

2.12. KA-induced Seizures Model Mice

Homozygous *Ryr1*^{C3636A} male mice and age-matched wild-type male littermates were used. Intraperitoneal injection of KA (40 mg kg^{-1}) in sterilized PBS was used to induce an SE at postnatal 8–12 weeks. Dantrolene (10 mg kg^{-1} body weight) in sterilized water was intraperitoneally injected 30 min after KA injection, when required. KA injection was carried out between 1 p.m. and 5 p.m. Animals were observed in the home cage and classified according to the seizure scale: (0) no response; (1) staring, rigid posture with straight and rigid tail; (2) head nodding, rearing and repetitive movement; (3) jumping, wobbling and/or falling; (4) non-intermittent seizure activity persisting for 30 min; (5) death. Only animals reaching at least stage 3–4 were considered for this study (38/72).

For light microscopic analysis, mice were anesthetized and perfused with 4% (*w*/*v*) paraformaldehyde in PBS 24 h after KA administration. Brains were removed and post-fixed with 4% paraformaldehyde in PBS overnight at 4 °C. Brains were cryoprotected by sequential immersion in 15 and then 30% (*w*/*v*) sucrose/PBS, and then embedded in Tissue Freezing Medium (Leica Microsystems). Sections were cut to 25-μm thickness using a cryostat (CM1900, Leica Instruments, Nussloch, Germany) at −20 °C. Tissue slices were mounted on PlatinumPro-coated slides (Matsunami, Osaka, Japan) and dried.

Slides were incubated in 0.1% (*w*/*v*) cresyl violet acetate (MP Biomedicals, Solon, OH, USA) and 0.1% (*v*/v) acetic acid for 5 min, followed by dehydration in ascending ratios of ethanol and xylene, and coverslipped with Malinol mounting medium (Muto Pure Chemicals, Tokyo, Japan).

2.13. Fluoro-Jade C Staining

Hippocampal cryo-sections were immersed in a solution of 5% (*w*/*v*) NaOH in 80% (*v*/v) ethanol for 5 min, then sequentially transferred to 70% (*v*/v) ethanol for 2 min, distilled water for 2 min, 0.06% (*w*/*v*) potassium permanganate for 10 min, and distilled water for 2 min at RT. Slices were then incubated for 20 min with 0.0002% (*w*/*v*) Fluoro-Jade C (Merck Millipore) (Schmued et al., 2005) and 2 μM DAPI in a 0.1% (*v*/v) acetic acid, and rinsed by three washes with distilled water. Sections were dried at 50 °C, dehydrated in xylene, and mounted with DPX Mountant (Sigma-Aldrich). Images of the hippocampal region were captured with a Leica TCS SP8 laser-scanning microscope equipped with a 10× objective. To quantify Fluoro-Jade C-positive cells, four mice per condition were used. For each hippocampus, six sections were analyzed. Neuronal degeneration was expressed as the intensity of CA3 fluorescence divided by that of CA1 fluorescence in the pyramidal cell layer.

2.14. [^{3}H]Ryanodine Binding Assay

Microsomes were prepared from forelimb and hindlimb muscles of adult mice. [^{3}H]Ryanodine binding assay was carried out based on a previously described procedure with some modifications (Murayama et al., 2015). Briefly, microsomes were incubated with 5 nM [^{3}*H*]ryanodine in a buffer containing 0.17 M NaCl, 20 mM 2-Hydroxy-3-morpholinopropanesulfonic acid (MOPSO), pH 7.0, 2 mM DTT, 1 mM β,γ-methylene adenosine triphosphate (AMPPCP) and various concentrations of free Ca^{2+}. The protein-bound [^{3}H]ryanodine was separated by filtering through polyethyleneimine-treated glass filters (Whatman GF/B; GE Helthcare) using Micro 96 Cell Harvester (Molecular Device, Sunnyvale, CA, USA). Nonspecific binding was determined in the presence of 20 μM unlabeled ryanodine. The [^{3}H]ryanodine binding data (*B*) were normalized to the maximal binding sites for [^{3}H]ryanodine (B_{max}) that was separately determined by Scatchard plot analysis using varied concentrations of [^{3}H]ryanodine (3–40 nM).

2.15. Vector Construction and Lentivirus Production

The coding sequence of TagRFP (Evrogen JSC, Moscow, Russia) (Merzlyak et al., 2007) with the mitochondrial targeting sequence was expressed by the mouse excitatory neuron-specific *Camk2a* promoter (pLenti-*Camk2a*-mito-TagRFP). Human embryonic kidney 293T (HEK293T) cells were cultured in DMEM supplemented with 5% (*v*/v) FBS, penicillin (100 units mL^{-1}), streptomycin (100 units mL^{-1}) and 8 mM L-glutamine. When HEK293T cells were grown to 90% confluence, culture medium was replaced with DMEM without antibiotics. Lentiviruses were produced by reverse transfection of HEK293T cells using 15 μg lentiviral vectors, 4 μg plasmids expressing the vesicular stomatitis virus glycoprotein (VSV-G), 8 μg packing plasmids Δ8.9 and Lipofectamine 2000 (Thermo Fisher Scientific) in 10 cm collagen type I-coated dishes (Asahi glass, Tokyo, Japan). Cells were incubated at 37 °C under 5% CO_2. After 15 h, the medium was replaced with fresh media and cells were incubated for 36 h at 32 °C. The lentivirus-containing medium was collected and cleared by centrifugation at 1500 rpm for 5 min (Centrifuge 5702, Eppendorf, Hamburg, Germany). For concentration of lentivirus, centrifugation was performed at 10,000 rpm overnight at 4 °C using microcentrifuge (Tomy, MRX-150). Supernatant was completely removed and virus pellets resuspended in 50 μL PBS and stored at −80 °C until use.

2.16. Analysis of Mitochondrial Circularity in Neurons

Primary cultured neurons at 4 d *in vitro* were infected with lentiviral mito-TagRFP. Four days after lentiviral infection, neurons were examined for morphological change of mitochondria. For the assessment of mitochondrial fragmentation, mitochondrial circularity (4π [area]/[perimeter]^2) was analyzed using ImageJ64 software (National Institute of Health, Bethesda, MD, U.S.A.).

2.17. Statistics

All statistical analyses of the data were performed using Microsoft Excel 2004 for Mac (Microsoft, Redmond, WA, USA) with the add-in software Statcel2 (OMS, Saitama, Japan). Differences between two groups were analyzed with Student's *t*-test. Differences between three or more groups were analyzed by ANOVA. *Post hoc* multiple comparisons were made using the Tukey-Kramer test.

3. Results

3.1. Generation and Characterization of NICR-deficient Mice

To examine the potential pathophysiological significance of NICR *in vivo*, we generated a mouse line *Ryr1*^{C3636A} in which the cysteine residue (Cys3636) critical for NICR (Kakizawa et al., 2012; Sun et al., 2001) is replaced by alanine residue (Fig. 1a and b). The *Ryr1*^{C3636A} mice exhibited no significant change in the body weight, gross anatomy of the brain or the protein levels of RyR1 or nNOS in the hippocampus and cerebral cortex (Fig. S1a–S1d). Moreover, there was no significant difference in the protein levels of RyR1 or nNOS, the ryanodine binding of sarcoplasmic reticulum fractions, which reflects CICR activity of RyRs (Meissner, 1994; Ogawa, 1994), or in depolarization-induced Ca^{2+} release *via* RyR1 in skeletal myocytes (Fig. S2a–S2e). When we compared the effect of caffeine, which is an agonist of CICR, on CICR in *Ryr1*^{C3636A} and *Ryr1*^{WT} neurons, we observed no significant difference (Fig. S3a and S3b). However, when we compared the effect of NOC7, an NO donor, on $[Ca^{2+}]_i$ in *Ryr1*^{C3636A} and *Ryr1*^{WT} neurons, we observed a marked increase in $[Ca^{2+}]_i$ only in *Ryr1*^{WT} neurons (Fig. 1c). Moreover, when we applied 50 μM *N*-methyl-D-aspartic acid (NMDA) to hippocampal slice cultures for 2 h to induce seizure-like activity, we found significant increases in *S*-nitrosylation of RyR1 in *Ryr1*^{WT} mice but not in *Ryr1*^{C3636A} mice (Fig. 1d), although NMDA-induced NO production was similarly observed in both *Ryr1*^{WT} and *Ryr1*^{C3636A} neurons (Fig. S3c and S3d). Collectively, these results indicate that in *Ryr1*^{C3636A} mice, Ca^{2+} release induced by NO is silenced, but other Ca^{2+} release modes *via* RyR1 are not.

3.2. Kainic Acid-induced Neuronal Cell Death in the Hippocampus was Reduced in the *Ryr1*^{C3636A} Mice

Prompted by our observation that NICR is genetically silenced in *Ryr1*^{C3636A} mice, we next studied the pathophysiological significance of NICR in the KA-induced temporal lobe epilepsy model (Nadler et al., 1978). KA induced severe seizure phenotype in both *Ryr1*^{WT} and *Ryr1*^{C3636A} mice (Fig. 2a). In *Ryr1*^{WT} mice, 24 h after KA administration, the CA3 region showed darkly stained shrunken pyramidal cells, indicative of neurodegeneration. In contrast, in KA-treated *Ryr1*^{C3636A} mice, the CA3 region was packed with large pyramidal cells similar to those found in sham-treated mice (Fig. 2b). These observations indicate that genetic inhibition of NICR ameliorates seizure-induced neurodegeneration, suggesting that pharmacological inhibition of NICR may also have a neuroprotective effect. Dantrolene is a well-known inhibitor of RyR1 at body temperature (Ohta and Endo, 1986). Indeed, we found that NICR was blocked by dantrolene in *Ryr1*^{WT} neurons at 37 °C (Fig. S3e). To examine whether dantrolene is protective against neurodegeneration caused by epileptic seizures *in vivo*, we administered dantrolene to *Ryr1*^{WT} and *Ryr1*^{C3636A} mice after KA-induced seizures. Although dantrolene had no significant effect on the maximum level of seizures (Fig. 2a), it circumvented morphological changes in the CA3 region in *Ryr1*^{WT} mice (Fig. 2b). In contrast, dantrolene administration had no apparent effect in *Ryr1*^{C3636A} mice.

We next examined the extent of seizure-induced neuronal damage using the neurodegeneration marker Fluoro-Jade C (FJC) (Schmued et al., 2005). FJC positve neurons were clearly visualized in CA3 region of KA-treated *Ryr1*^{WT} mice but scarcely observed in KA-treated *Ryr1*^{C3636A} mice, which showed similar staining as sham-treated animals (Fig. 2c). Moreover, 4′,6-Diamidino-2-phenylindole (DAPI) staining revealed cells with condensed, pyknotic nuclei, representative of apoptotic cells, in the CA3 region of KA-treated *Ryr1*^{WT} mice but not in *Ryr1*^{C3636A} mice (Fig. 2d). Thus, the hippocampus of *Ryr1*^{C3636A} mice deficient in NICR was protected from seizure-induced neurodegeneration. Furthermore, *in vivo* dantrolene administration reduced the amount of neurodegeneration analyzed using FJC staining in *Ryr1*^{WT} mice (Fig. 2c and d). In contrast, dantrolene treatment had no effect on *Ryr1*^{C3636A} mice. These results indicate that the NICR inhibitors such as dantrolene may have therapeutic potential for treating neurodegeneration after epileptic seizures.

3.3. NO-induced Neuronal Cell Death was Milder in the *Ryr1*^{C3636A} Neurons In Vitro

These *in vivo* results led us to study the role of NICR in NO-induced neuronal cell death. Five hours after the application of NOC7, *Ryr1*^{WT} cultured neurons showed a distinctive pattern of morphological changes characterized by short and curly neurites, whereas such shortening of neurites was absent in *Ryr1*^{C3636A} neurons (Fig. 3a). In *Ryr1*^{WT} neurons, dantrolene exerted a protective effect against NOC7-induced morphological changes. In contrast, no significant effect of dantrolene was detected in *Ryr1*^{C3636A} neurons (Fig. 3a).

We next examined the mitochondrial membrane potential ($\Delta\Psi_m$), which is dissipated in apoptotic cells, by using the JC-1 assay (Kroemer and Reed, 2000). In *Ryr1*^{WT} neurons exposed to NOC7, the red/green ratio of JC-1 decreased, indicative of reduced $\Delta\Psi_m$, whereas in *Ryr1*^{C3636A} neurons, the red/green ratio was sustained after NOC7 application (Fig. 3b). Thus, NO induced mitochondrial dysfunction in *Ryr1*^{WT} but not in *Ryr1*^{C3636A} neurons. Again, dantrolene reversed the NO-induced reduction of $\Delta\Psi_m$ in *Ryr1*^{WT} neurons, but had no significant effect in *Ryr1*^{C3636A} neurons (Fig. 3b).

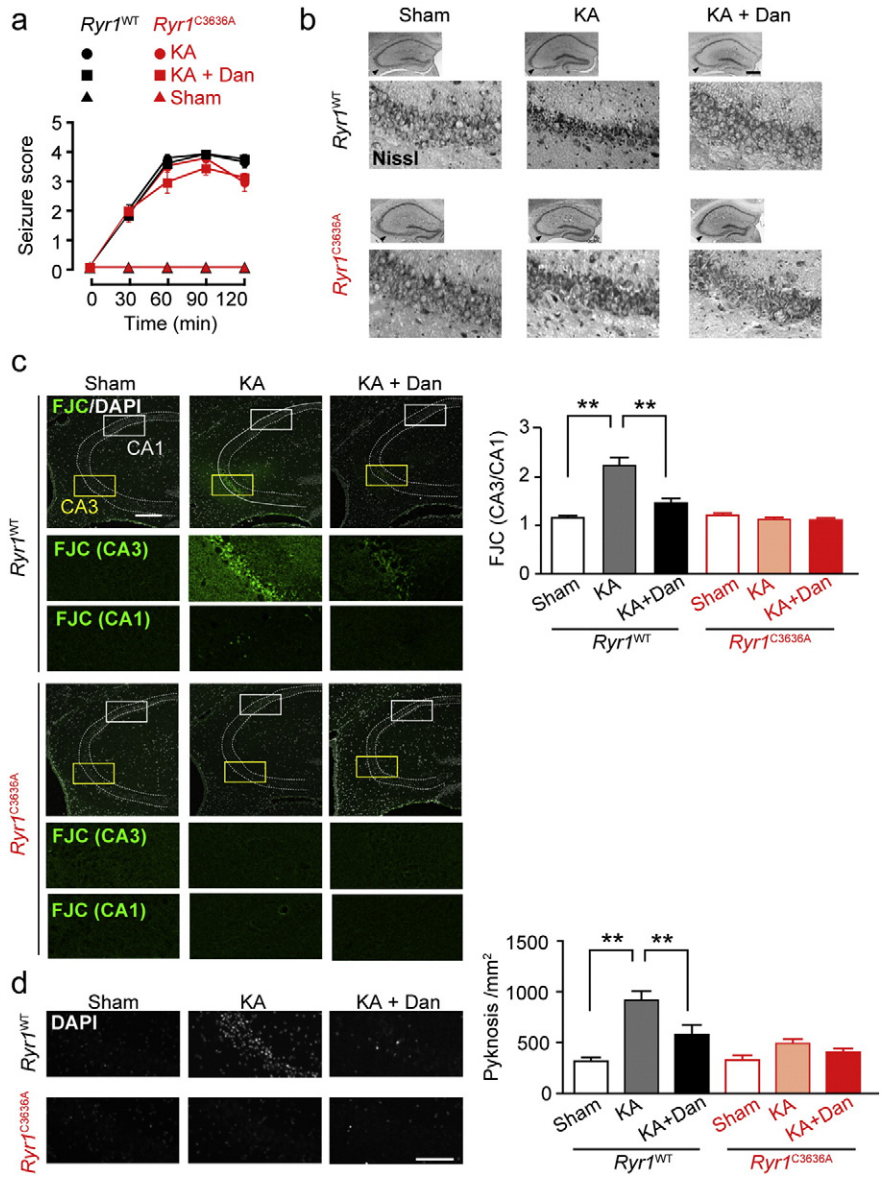

Fig. 2. Kainic acid-induced neurodegeneration in CA3 region was reduced in *Ryr1*^{C3636A} mice (a) KA (40 mg kg^{-1}, i.p.) triggered limbic seizures. n = 5–7. Dan, dantrolene. (b) Nissl-staining of hippocampus 24 h after KA injection. Scale bar: 500 μm. (c) Fluoro-Jade C staining of hippocampus. Dotted lines show the position of stratum pyramidale. Yellow (CA3) and white (CA1) boxed areas in upper panels are shown enlarged in bottom panels. n = 28–40 slices from 5 to 7 mice. Scale bar: 200 μm. Error bars indicate s.e.m. Data are analyzed for significance using ANOVA followed by a Tukey-Kramer *post-hoc* test. ** $p < 0.01$. (d) DAPI staining of hippocampus. n = 30–43 slices from 5 to 7 mice. Scale bar: 100 μm. Error bars indicate s.e.m. Data are analyzed for significance using ANOVA followed by a Tukey-Kramer *post-hoc* test. ** $p < 0.01$.

Mitochondrial fragmentation occurs early in apoptosis and plays a key role in cell death progression (Knott et al., 2008). We, therefore, carried out time-lapse imaging of the mitochondrial morphology in cultured neurons, in which mitochondria-targeted TagRFP was expressed. Upon application of 100 μM glutamate, which is known as a strong inducer of neuronal apoptosis (Choi, 1988), a significant increase in mitochondrial fragmentation was observed (Fig. 4 top left). Similarly, after NOC7 application, we observed a significant increase in mitochondrial fragmentation in *Ryr1*^{WT} neurons (Fig. 4 middle left). However, NOC7-induced mitochondrial fragmentation was scarcely observed in *Ryr1*^{C3636A} neurons (Fig. 4 bottom left). We quantified the mitochondrial fragmentation analyzing the circularity of the mitochondrial morphology (see Materials and methods). Although glutamate induced mitochondrial fragmentation in both *Ryr1*^{WT} and *Ryr1*^{C3636A} neurons to the same extent, NOC7 induced mitochondrial fragmentation only in *Ryr1*^{WT} neurons, and NOC7-induced mitochondrial fragmentation was absent in *Ryr1*^{C3636A} neurons (Fig. 4 right panels). We also examined the effect of dantrolene on NOC7-induced mitochondrial fragmentation, but did not find a significant effect of the drug (data not shown). These results suggest that neuronal cell death induced by NICR is accompanied by mitochondrial dysfunction, but the causal relationship requires further clarification.

NO may also exert its cytotoxic effect through the formation of peroxynitrite (Szabó et al., 2007). However, the peroxynitrite donor 3-morpholino-sydnonimine (SIN-1) induced neuronal cell death in both *Ryr1*^{WT} and *Ryr1*^{C3636A} neurons to the same extent (Fig. S4a and S4b). Thus, Cys3636 in RyR1 is unlikely to be the key residue affected by peroxynitrite.

4. Discussion

These results indicate the involvement of NICR in neurodegeneration following SE. Moreover, this data set is consistent with the finding that epileptic seizure-induced neurotoxicity is reduced in nNOS-

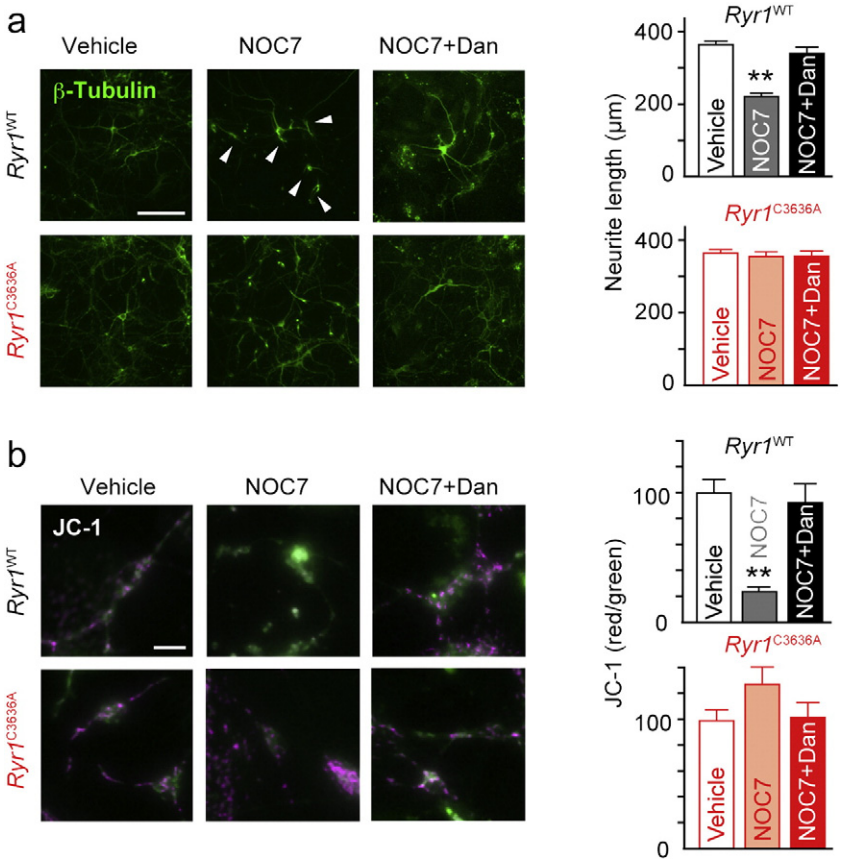

Fig. 3. Involvement of NICR in NO-induced neuronal cell death (a) Effect of NO on neuron morphology (stained with *anti*-β-III tubulin antibody). Arrowheads indicate short and curly neurites. Scale bar: 100 μm. Graphs show the length of the longest neurite of each neuron; n = 52–116; error bars indicate s.e.m. Concentrations of NOC7 and dantrolene (Dan) were 500 μM and 10 μM, respectively. Data were analyzed for significance using ANOVA followed by a Tukey-Kramer *post-hoc* test. ** $p < 0.01$. (b) Cell viability examined by JC-1 assay. Scale bar: 10 μm. n = 49–65. Error bars indicate s.e.m. Data were analyzed for significance using ANOVA followed by a Tukey-Kramer *post-hoc* test. ** $p < 0.01$. See also Fig. S4.

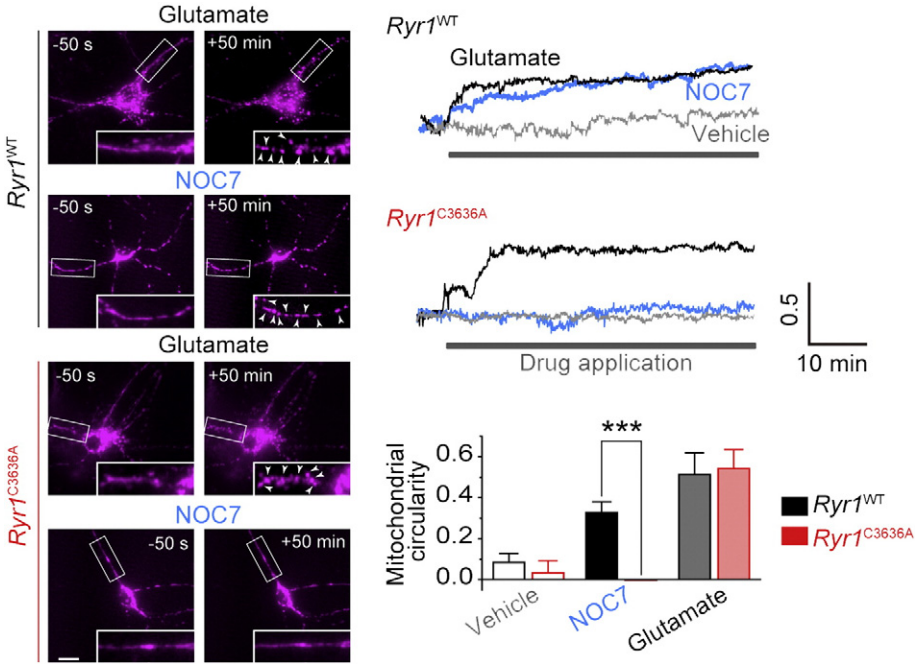

Fig. 4. Involvement of NICR in NO-induced mitochondrial fragmentation. Left panels show mitochondrial morphology before and 50 min after drug application. Glutamate (Glu; 100 μM) was used in positive control experiments. NOC7 concentration was 500 μM. Right upper panels show the representative time courses of fragmentation assessed by circularity of mitochondria. Right bottom panel show the average circularity of mitochondria between 55 and 60 min after drug application. Scale bar: 5 μm. n = 10–16. Data are analyzed for significance using *t*-test. *** $p < 0.001$.

deficient mice (Parathath et al., 2007). Although the targets of NO have been elusive, the present results highlight the importance of the *S*-nitrosylation of RyR1 at Cys3636 (corresponding to Cys3635 in rabbits and humans). This cysteine residue has been shown to undergo various redox modifications such as oxidation by H_2O_2 and *S*-glutathionylation in addition to *S*-nitrosylation (Aracena-Parks et al., 2006). However, H_2O_2 has been shown to activate both rabbit $RyR1^{WT}$ and $RyR1^{C3635A}$ (Aracena-Parks et al., 2006). Furthermore, while it was reported that *S*-nitrosoglutathione (GSNO) preferentially *S*-glutathionylated Cys3635 (Aracena-Parks et al., 2006), another study found that GSNO activated $RyR1^{C3635A}$ similarly to $RyR1^{WT}$ (Sun et al., 2003). Thus, neither oxidation nor *S*-glutathionylation of Cys3636 is likely to be involved in the activation of RyR1.

The RyR1 antagonist dantrolene is an approved drug for the treatment of malignant hyperthermia, which is a pharmacogenetic disorder in patients characterized by an increased susceptibility of muscular RyR1 to general anesthetics (Hirshey Dirksen et al., 2011). Several studies have raised the possibility of dantrolene as a treatment for neurodegeneration (Mody and MacDonald, 1995; Muehlschlegel and Sims, 2009). However, the precise mechanism for its therapeutic effect has remained elusive. The present results shed light on this important question, and pave the way for exploring RyR1 antagonists as therapeutics for brain damage associated with epileptic seizures.

NO is implicated in various other pathological conditions in the brain, including excitotoxicity during ischemic brain injury (Nakamura et al., 2013; Pacher et al., 2007). For instance, in the middle cerebral artery occlusion model, the brain injury is milder in mice treated with an nNOS-specific inhibitor and in nNOS-deficient mice (Huang et al., 1994). Thus, it seems possible that NICR may also play a role in ischemic brain injury (Kakizawa et al., 2012), and that RyR1 antagonist may have a potential therapeutic value in other neurodegenerative diseases associated with excitotoxicity.

Author Contributions

MI and SK conceived the research; YM, KK, YO and MI designed the research; YM, KK, TN and TM carried out the experiments; KS, HS, RK, AI, TY, YI, TS, NS and SK provided experimental tools; YM, KK, YO, TN, JS, TM and MI analyzed the data; YM and MI wrote the manuscript; and MI supervised the study.

Abbreviations

AM	acetoxymethyl ester
CHAPS	3-[(3-cholamidopropyl)dimethylammonio]-1-propanesulfonate
CICR	Ca^{2+}-induced Ca^{2+} release
Dan	dantrolene
DAPI	4′,6-Diamidino-2-phenylindole
DAR-4M	Diaminorhodamine-4M
DMEM	Dulbecco's modified Eagle medium
DTT	dithiothreitol
EDTA	ethylenediaminetetraacetic acid
ER	endoplasmic reticulum
ES	embryonic stem
FBS	fetal bovine serum
FGF	fibroblast growth factor
FJC	Fluoro-Jade C
GAPDH	glyceraldehyde 3-phosphate dehydrogenase
GSNO	*S*-nitrosoglutathione
HEK	human embryonic kidney
HEPES	2-[4-(2-Hydroxyethyl)-1-piperazinyl]ethanesulfonic acid
HRP	horseradish peroxidase
KA	kainic acid
JC-1	J-aggregate forming lipophilic cation 5,5′,6,6′-tetrachloro-1,1′,3,3′-tetraethyl-benzimidazolcarbocyanine iodide
MK-801	(5*S*,10*R*)-(+)-5-Methyl-10,11-dihydro-5*H*-dibenzo[*a*,*d*]cyclohepten-5,10-imine maleate
NA	numerical aperture
NICR	nitric oxide-induced Ca^{2+} release
NMDA	*N*-methyl-D-aspartic acid
NEM	*N*-ethylmaleimide
nNOS	neuronal nitric oxide synthase
NO	nitric oxide
NOC7	1-hydroxy-2-oxo-3-(*N*-methyl-3-aminopropyl)-3-methyl-1-triazene
NOS	nitric oxide synthase
NP-40	Nonidet P 40
PBS	phosphate-buffered saline
PVDF	polyvinylidene fluoride
ROI	regions of interest
RT	room temperature
RyR1	type 1 ryanodine receptor
SDS	sodium dodecyl sulfate
SE	status epilepticus
SIN-1	3-morpholino-sydnonimine
TBS	tris-buffered saline
$\Delta\Psi_m$	mitochondrial membrane potential

Acknowledgement

We thank Dr. Masahiko Watanabe for providing rabbit *anti*-RyR1 antibody and Mr. Yasuhiro Oda for technical assistance. This work was supported by JSPS KAKENHI Grant Number JP21229004 and JP25221304 to MI, JP13J00025 and JP15K08227 to YM, JP15H05648 to KK and JP23659037 and JP15K06774 to SK, and grants from Takeda Science Foundation and Mochida Memorial Foundation to SK.

The authors have declared that no conflict of interest exists.

Appendix A. Supplementary Data

Supplementary data to this article can be found online at http://dx.doi.org/10.1016/j.ebiom.2016.08.020.

References

Aghdasi, B., Reid, M.B., Hamilton, S.L., 1997. Nitric oxide protects the skeletal muscle Ca^{2+} release channel from oxidation induced activation. J. Biol. Chem. 272, 25462–25467.

Aracena-Parks, P., Goonasekera, S.A., Gilman, C.P., Dirksen, R.T., Hidalgo, C., Hamilton, S.L., 2006. Identification of cysteines involved in *S*-nitrosylation, *S*-glutathionylation, and oxidation to disulfides in ryanodine receptor type 1. J. Biol. Chem. 281, 40354–40368.

Bellinger, A.M., Reiken, S., Carlson, C., Mongillo, M., Liu, X., Rothman, L., Matecki, S., Lacampagne, A., Marks, A.R., 2009. Hypernitrosylated ryanodine receptor calcium release channels are leaky in dystrophic muscle. Nat. Med. 15, 325–330.

Berkovic, S.F., Mulley, J.C., Scheffer, I.E., Petrou, S., 2006. Human epilepsies: interaction of genetic and acquired factors. Trends Neurosci. 29, 391–397.

Betjemann, J.P., Lowenstein, D.H., 2015. Status epilepticus in adults. Lancet Neurol. 14, 615–624.

Chang, B.S., Lowenstein, D.H., 2003. Epilepsy. N. Engl. J. Med. 349, 1257–1266.

Choi, D.W., 1988. Glutamate neurotoxicity and diseases of the nervous system. Neuron 1, 623–634.

Durham, W.J., Aracena-Parks, P., Long, C., Rossi, A.E., Goonasekera, S.A., Boncompagni, S., Galvan, D.L., Gilman, C.P., Baker, M.R., Shirokova, N., et al., 2008. RyR1 *S*-nitrosylation underlies environmental heat stroke and sudden death in Y522S RyR1 knockin mice. Cell 133, 53–65.

Eu, J.P., Sun, J., Xu, L., Stamler, J.S., Meissner, G., 2000. The skeletal muscle calcium release channel: coupled O_2 sensor and NO signaling functions. Cell 102, 499–509.

Goldberg, E.M., Coulter, D.A., 2013. Mechanisms of epileptogenesis: a convergence on neural circuit dysfunction. Nat. Rev. Neurosci. 14, 337–349.

Grynkiewicz, G., Poenie, M., Tsien, R.Y., 1985. A new generation of Ca^{2+} indicators with greatly improved fluorescence properties. J. Biol. Chem. 260, 3440–3450.

Hess, D.T., Matsumoto, A., Kim, S.O., Marshall, H.E., Stamler, J.S., 2005. Protein *S*-nitrosylation: purview and parameters. Nat. Rev. Mol. Cell. Biol. 6, 150–166.

Hirshey Dirksen, S.J., Larach, M.G., Rosenberg, H., Brandom, B.W., Parness, J., Lang, R.S., Gangadharan, M., Pezalski, T., 2011. Future directions in malignant hyperthermia research and patient care. Anesth. Analg. 113, 1108–1119.

Huang, Z., Huang, P.L., Panahian, N., Dalkara, T., Fishman, M.C., Moskowitz, M.A., 1994. Effects of cerebral ischemia in mice deficient in neuronal nitric oxide synthase. Science 265, 1883–1885.

Jaffrey, S.R., Erdjument-Bromage, H., Ferris, C.D., Tempst, P., Snyder, S.H., 2001. Protein *S*-nitrosylation: a physiological signal for neuronal nitric oxide. Nat. Cell Biol. 3, 193–197.
Jentsch, T.J., Hubner, C.A., Fuhrmann, J.C., 2004. Ion channels: function unravelled by dysfunction. Nat. Cell Biol. 6, 1039–1047.
Kakizawa, S., Kishimoto, Y., Hashimoto, K., Miyazaki, T., Furutani, K., Shimizu, H., Fukaya, M., Nishi, M., Sakagami, H., Ikeda, A., Kondo, H., Watanabe, M., Iino, M., Takeshima, H., 2007. Junctophilin-mediated channel crosstalk essential for cerebellar synaptic plasticity. EMBO J. 26, 1924–1933.
Kakizawa, S., Yamazawa, T., Chen, Y., Ito, A., Murayama, T., Oyamada, H., Kurebayashi, N., Sato, O., Watanabe, M., Mori, N., Oguchi, K., Sakurai, T., Takeshima, H., Saito, N., Iino, M., 2012. Nitric oxide-induced calcium release via ryanodine receptors regulates neuronal function. EMBO J. 31, 417–428.
Kanemaru, K., Okubo, Y., Hirose, K., Iino, M., 2007. Regulation of neurite growth by spontaneous Ca^{2+} oscillations in astrocytes. J. Neurosci. 27, 8957–8966.
Knott, A.B., Perkins, G., Schwarzenbacher, R., Bossy-Wetzel, E., 2008. Mitochondrial fragmentation in neurodegeneration. Nat. Rev. Neurosci. 9, 505–518.
Kojima, H., Hirotani, M., Nakatsubo, N., Kikuchi, K., Urano, Y., Higuchi, T., Hirata, Y., Nagano, T., 2001. Bioimaging of nitric oxide with fluorescent indicators based on the rhodamine chromophore. Anal. Chem. 73, 1967–1973.
Koyama, R., Muramatsu, R., Sasaki, T., Kimura, R., Ueyama, C., Tamura, M., Tamura, N., Ichikawa, J., Takahashi, N., Usami, A., et al., 2007. A low-cost method for brain slice cultures. J. Pharmacol. Sci. 104, 191–194.
Koyama, R., Tao, K., Sasaki, T., Ichikawa, J., Miyamoto, D., Muramatsu, R., Matsuki, N., Ikegaya, Y., 2012. GABAergic excitation after febrile seizures induces ectopic granule cells and adult epilepsy. Nat. Med. 18, 1271–1278.
Kroemer, G., Reed, J.C., 2000. Mitochondrial control of cell death. Nat. Med. 6, 513–519.
Meisler, M.H., Kearney, J.A., 2005. Sodium channel mutations in epilepsy and other neurological disorders. J. Clin. Invest. 115, 2010–2017.
Meissner, G., 1994. Ryanodine receptor/Ca^{2+} release channels and their regulation by endogenous effectors. Annu. Rev. Physiol. 56, 485–508.
Merzlyak, E.M., Goedhart, J., Shcherbo, D., Bulina, M.E., Shcheglov, A.S., Fradkov, A.F., Gaintzeva, A., Lukyanov, K.A., Lukyanov, S., Gadella, T.W., et al., 2007. Bright monomeric red fluorescent protein with an extended fluorescence lifetime. Nat. Methods 4, 555–557.
Mody, I., MacDonald, J.F., 1995. NMDA receptor-dependent excitotoxicity: the role of intracellular Ca^{2+} release. Trends Pharmacol. Sci. 16, 356–359.
Muehlschlegel, S., Sims, J.R., 2009. Dantrolene: mechanisms of neuroprotection and possible clinical applications in the neurointensive care unit. Neurocrit. Care. 10, 103–115.
Mülsch, A., Busse, R., Mordvintcev, P.I., Vanin, A.F., Nielsen, E.O., Scheel-Krüger, J., Olesen, S.P., 1994. Nitric oxide promotes seizure activity in kainate-treated rats. Neuroreport 5, 2325–2328.
Murayama, T., Kurebayashi, N., Yamazawa, T., Oyamada, H., Suzuki, J., Kanemaru, K., Oguchi, K., Iino, M., Sakurai, T., 2015. Divergent activity profiles of type 1 ryanodine receptor channels carrying malignant hyperthermia and central core disease mutations in the amino-terminal region. PLoS One 10, e0130606.
Nadler, J.V., Perry, B.W., Cotman, C.W., 1978. Intraventricular kainic acid preferentially destroys hippocampal pyramidal cells. Nature 271, 676–677.
Nakamura, T., Tu, S., Akhtar, M.W., Sunico, C.R., Okamoto, S., Lipton, S.A., 2013. Aberrant protein *S*-nitrosylation in neurodegenerative diseases. Neuron 78, 596–614.
Ogawa, Y., 1994. Role of ryanodine receptors. Crit. Rev. Biochem. Mol. Biol. 29, 229–274.
Ohta, T., Endo, M., 1986. Inhibition of calcium-induced calcium release by dantrolene at mammalian body-temperature. Proc. Jpn. Acad. Ser. B Phys. Biol. Sci. 62, 329–332.
Pacher, P., Beckman, J.S., Liaudet, L., 2007. Nitric oxide and peroxynitrite in health and disease. Physiol. Rev. 87, 315–424.
Parathath, S.R., Gravanis, I., Tsirka, S.E., 2007. Nitric oxide synthase isoforms undertake unique roles during excitotoxicity. Stroke 38, 1938–1945.
Rando, T.A., Blau, H.M., 1994. Primary mouse myoblast purification, characterization, and transplantation for cell-mediated gene therapy. J. Cell Biol. 125, 1275–1287.
Schmued, L.C., Stowers, C.C., Scallet, A.C., Xu, L., 2005. Fluoro-Jade C results in ultra high resolution and contrast labeling of degenerating neurons. Brain Res. 1035, 24–31.
Sun, J., Xin, C., Eu, J.P., Stamler, J.S., Meissner, G., 2001. Cysteine-3635 is responsible for skeletal muscle ryanodine receptor modulation by NO. Proc. Natl. Acad. Sci. U. S. A. 98, 11158–11162.
Sun, J., Xu, L., Eu, J.P., Stamler, J.S., Meissner, G., 2003. Nitric oxide, NOC-12, and *S*-nitrosoglutathione modulate the skeletal muscle calcium release channel/ryanodine receptor by different mechanisms. An allosteric function for O_2 in *S*-nitrosylation of the channel. J. Biol. Chem. 278, 8184–8189.
Szabó, C., Ischiropoulos, H., Radi, R., 2007. Peroxynitrite: biochemistry, pathophysiology and development of therapeutics. Nat. Rev. Drug Discov. 6, 662–680.